Supplementary Information to

Migration of the Antarctic Polar Front over the last glacial cycle

Lena M. Thöle[1, 2, 3†*], Xuyuan E. Ai[2, 4†*], Alexandra Auderset[2], Mareike Schmitt[2], Simone Moretti[2], Anja S. Studer[2, 5], Elisabeth Michel[6], Martin Wegmann[7], Alain Mazaud[6], Peter K. Bijl[3], Daniel M. Sigman[4], Alfredo Martínez-García[2], Samuel L. Jaccard[1,8*]

[1]Institute of Geological Sciences and Oeschger Centre for Climate Change Research, University of Bern, Bern, Switzerland.
[2]Max Planck Institute for Chemistry, Climate Geochemistry Department, Mainz, Germany.
[3]Marine Palynology and Paleoceanography, Department of Earth Sciences, Utrecht University, The Netherlands.
[4]Department of Geosciences, Princeton University, Princeton, NJ, USA.
[5]Aquatic and Isotope Biogeochemistry, Department of Environmental Sciences, University of Basel, Switzerland.
[6]Laboratoire de Sciences et de l'Environnement (LSCE), Gif-sur-Yvette, France.
[7]Institute of Geography and Oeschger Centre for Climate Change Research, University of Bern, Bern, Switzerland.
[8]Institute of Earth Sciences, University of Lausanne, Lausanne, Switzerland.
[†]Contributed equally to this work
[*]Corresponding authors: Lena M. Thöle (l.m.thole@uu.nl), Xuyuan E. Ai (xuyuana@princeton.edu), & Samuel L. Jaccard (Samuel.jaccard@unil.ch)

This document includes:

Supplementary Text
Supplementary Figure 1-16
Supplementary References

Supplementary Text

Comparison of TEX_{86} and TEX^L_{86} temperature calibration

The comparison of the TEX_{86} and TEX^L_{86} indices with the EPICA Dome C (EDC) δD record depicts similar trends and an equally good correlation between the two indices in cores MD11-3357 (Supplementary Fig. 1a). However, the reconstruction for core MD11-3353 shows the tight correlation between TEX^L_{86} and the deuterium record (Supplementary Fig. 1b), whereas the TEX_{86} values fail to record a distinct glacial–interglacial pattern, and overall do not depict a strong correlation with the deuterium record. Independent of the calibration used, TEX^L_{86} SST reconstructions correlate better with Antarctic δD air temperatures than does TEX_{86}. The main difference between these indices is that the TEX^L_{86} index excludes the crenarchaeol regioisomer, which is found only in low abundances in cold polar environments, particularly when temperatures fall below 8ºC[1]. Hence, in this study we decided to use the TEX^L_{86} calibration in ref. 2 to reconstruct changes in SST (Supplementary Fig. 2). Reconstructed core-top SST values are slightly warmer compared to modern values[3], yet they remain in the error range of the TEX^L_{86} calibration. Generally, the TEX^L_{86} calibrations have proven robust for cold environments[1,2,4], with the absolute error relative to the temperature calibration amounts to ± 2.8°C[2,5]. However, local as well as downcore uncertainties can be much smaller[5]. Hence, we are confident that the calibration provides SST estimates that are internally consistent and allow for reliable glacial-interglacial reconstructions despite the potential discrepancy with modern SST data.

We use the Methane Index[6], the BIT index[7], the %GDGT-0 index[8], the 2/3 ratio[9] and the Ring Index[10] to assess potential contributions of non-pelagic GDGT sources to the sedimentary signal (Supplementary Fig. 3). The values obtained for those indices are within the expected range for marine Thaumarcheota and allow for the use of GDGT-based SST reconstruction.

Resampling of SST data

The average original resolution for the cores is 1,500 years for MD11-3353 and 1,600 years for MD11-3357, but lowest resolution is briefly up to 5,000 years for MD11-3353 (during MIS 5 and 6) and MD11-3357 (during MIS 5). The resampling resolution, 2,500 years, was chosen to stay as close to the original cores' resolutions as possible and to not introduce too many or too few sample points. Tests with different resampling resolutions have shown no change in the glacial-interglacial pattern of the SST difference (ΔSST) (Supplementary Fig. 4). To test our approach, we also calculated the running average on a 3-, 5- and 7-step resolution and used a Monte Carlo and Kalman filter method to calculate the mean SST records and ΔSST records, taking into account the age model uncertainty of the two records (1σ = 2,000 years)[11]. All approaches show similar results for individual cores as well as for the ΔSST calculation (see Supplementary Fig. 4).

Sensitivity analysis of the quantitative model

To evaluate how the major parameters of the quantitative framework, $range_{AZ}$ (i.e., the maximum temperature change in the Antarctic Zone (AZ)), $range_{SAZ}$ (i.e., the maximum temperature change in the Subantarctic Zone (SAZ)), and a (i.e., the linear factor between Δlat and ΔT_{EDC}) affect the simulated ΔSST between the two core sites, we did a series of sensitivity tests. To show a more complete or even exaggerated range of latitudinal frontal shift, we extend the assumed EDC temperature change to [-15 15] °C. However, $range_{AZ}$ and $range_{SAZ}$ still represent the range of temperature change for the last 150,000 years at EDC. Hence, when the assumed ΔT_{EDC} falls outside of the EDC temperature of the last 150,000 years, the actual change in the SST profile of the respective regions will be larger than $range_{AZ}$ or $range_{SAZ}$.

First, we varied a between 0 and 1, while keeping $b = 0$ for simplicity. We repeated these experiments for different combinations of realistic values for $range_{AZ}$ and $range_{SAZ}$ (Supplementary Fig. 6). The results show that regardless of $range_{AZ}$ and $range_{SAZ}$, the ΔSST between the two sites will have a non-monotonic horse-shoe pattern only when a ≠ 0, that is when the latitude of the polar front (PF) varies with Antarctic climate. When there is no polar frontal shift, the ΔSST between the two sites will unidirectionally decrease ($range_{AZ} > range_{SAZ}$), increase ($range_{AZ} < range_{SAZ}$) or remain stable ($range_{AZ} = range_{SAZ}$). Changes in a, $range_{AZ}$ and $range_{SAZ}$ changes the shape of the horse-shoe pattern.

When the ΔSST between the two sites are plotted over the amount of latitudinal shift, we can see that except in the scenario where a is 0.25, the values of latitudinal shift for the largest ΔSST are similar, around 1.7-2° poleward (Supplementary Fig. 7), suggesting that it is the latitudinal shift, not the differential warming/cooling of the AZ and SAZ, that dominates the changes in ΔSST between the two sites. This is due to the fact that site MD11-3357 is currently ~1.8° south of $lat2$, the boundary between the Polar Frontal Zone (PFZ) and the SAZ, and site MD11-3353 is ~1.9° south of $lat1$, the boundary between the AZ and the PFZ. When a is relatively large, a southward shift of 1.8-1.9° of the PF from its current latitude will place a greater fraction of the steep PFZ SST profile between the two sites, leading to a maximum ΔSST. In the model setup, because the position of $lat1$ and $lat2$ relative to each other remain unchanged, the latitudinal shift that produces the maximum ΔSST would be the same. However, the changing slope of the PFZ SST line brings some variance to the exact value of the maximum ΔSST. When a is very small, the southward shift of the polar front is too slow relative to the decrease in the SST slope of the PFZ segment that accompanies warming. As a result, when a southward shift of ~1.8-1.9° happens, the temperature difference between the AZ and the SAZ is too small, that although a greater fraction of the PF SST slope is placed between the two sites, the resulting ΔSST between MD11-3357 and MD11-3353 is still smaller than that in the initial scenario. Nevertheless, the ΔSST starts to drop much faster when the PF is shifting further poleward of this position, suggesting that the latitudinal position of the polar front still has large impacts on the ΔSST between MD11-3353 and MD11-3357.

If we only consider relatively large values for a, the maximum ΔSST between the two sites would occur when the PF is ~1.8° southward of its current position, and we can use the following equation to calculate the EDC temperature change corresponding to the maximum SST gradient between the two sites:

$$\Delta lat(\max SSTgrad) = a * \Delta T_{EDC} + b = 1.8$$

$$\Delta T_{EDC}(\max SSTgrad) = \frac{1.8 - b}{a}$$

For $b < 1.8$, $\Delta T_{EDC}(\max SSTgrad) > 0$, and $\Delta T_{EDC}(\max SSTgrad)$ decreases when a increases (Supplementary Fig. 6). For $b > 1.8$, $\Delta T_{EDC}(\max SSTgrad) < 0$, and $\Delta T_{EDC}(\max SSTgrad)$ increases when a increases (Supplementary Fig. 9).

The maximum SST gradient between MD11-3357 and MD11-3353 depends on whether $\Delta T_{EDC}(\max SSTgrad)$ is negative or positive, and whether $range_{AZ}$ is larger than $range_{SAZ}$. If $\Delta T_{EDC}(\max SSTgrad) > 0$, it means that the largest SST gradient occurs when the climate is warmer than the present. If $range_{AZ}$ is larger than $range_{SAZ}$, the temperature changes in the two regions would follow "polar amplification", which means that global warming corresponds to a smaller temperature difference between the AZ and the SAZ and a less steep PFZ SST segment. When a decreases, $\Delta T_{EDC}(\max SSTgrad)$ becomes larger, resulting a less steep slope of the PF SST segment at the time of maximum SST gradient and a smaller maximum SST gradient between the two sites (Supplementary figs. 6(a) and 8). If $range_{AZ}$ is smaller than $range_{SAZ}$, the temperature changes in the two regions follows "tropical amplification". Global warming corresponds to a larger temperature difference between the AZ and the SAZ and a steeper slope of the PFZ SST segment. In this case, when a decreases, $\Delta T_{EDC}(\max SSTgrad)$ becomes larger, which means a steeper slope of the PF SST segment, and greater maximum SST gradient between the two sites (Supplementary Figs. 6(b) and 8).

On the other hand, if $\Delta T_{EDC}(\max SSTgrad) < 0$, the largest SST gradient occurs when the climate is cooler than the present. If $range_{AZ}$ is larger than $range_{SAZ}$ ("polar amplification"), the cooler the EDC temperature, the steeper the slope of the PF SST segment line. When a decreases, $\Delta T_{EDC}(\max SSTgrad)$ becomes more negative, which means a steeper slope of the PF SST segment, and a greater maximum SST gradient between the two sites (Supplementary Figs. 9(a) and 11). If

$range_{AZ}$ is smaller than $range_{SAZ}$ ("tropical amplification"), a cooler global temperature means a less steep PF SST segment line. When a decreases, $\Delta T_{EDC}(\max SSTgrad)$ becomes more negative, leading to a small maximum SST gradient between the two sites (Supplementary figs. 9(b) and11).

The impacts of different $range_{AZ}$ and $range_{SAZ}$ on optimal model parameters

There are different estimates from literature for maximum SST change in the AZ and the SAZ. In the SST compilation of ref. 12, the SST of 50° to 60°S ranges from 5.1°C to 1.6°C. The MARGO Last Glacial Maximum global temperature reconstruction shows that the AZ was ~2-4°C cooler than the present and the mid latitude was 0-2°C cooler than the present in the Indian Ocean[13]. We took $range_{AZ} = 3$°C and $range_{SAZ} = 1$°C in our optimized simulation. The sensitivity analysis shows that $range_{AZ}$, and $range_{SAZ}$ has little impact on when the maximum SST gradient occurs. The values of the best fitting a' and b' vary slightly with different values for $range_{AZ}$, and $range_{SAZ}$. When we reverse the values for $range_{AZ}$ and $range_{SAZ}$, that is when $range_{AZ}$ = 1°C, and $range_{SAZ} = 3$°C, the best-fitting a' is slightly larger at ~0.68, and the best-fitting b' becomes ~0.78 (Supplementary Fig. 14). This produces a polar front that is ~5.3° southward of its current location when the EDC temperature change is 0°C, comparing to a polar front ~4.33° southward of its current location when the EDC temperature change is 0°C, if $range_{AZ}$ = 3°C, and $range_{SAZ} = 1$°C. Considering the uncertainty in both the chronology and the SST value of the TEX^L_{86}-reconstructed data, the differences in calculated optimal a' and b' between different choices of $range_{AZ}$ and $range_{SAZ}$ are small. Reversing the values for $range_{AZ}$ and $range_{SAZ}$ is a big change in terms of setting the paleoclimate background of the model, and the similarity of the calculated optimal parameters suggests our quantitative model is robust. Thus $range_{AZ}$ and $range_{SAZ}$, the differential warming/cooling of the AZ and the SAZ, exerts limited influence on the trend of the SST gradient.

Supplementary Figures

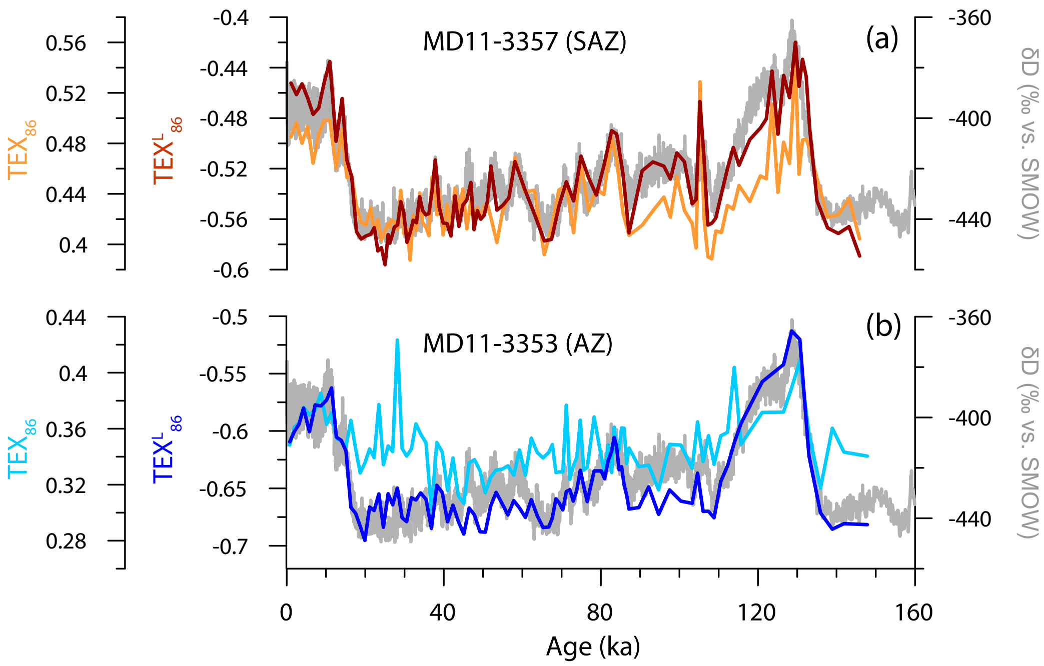

Supplementary Figure 1. Comparison of the TEX_{86} and TEX^{L}_{86} index for cores (a) MD11–3357 (SAZ) and (b) MD11–3353 (AZ) compared to the EDC δD record[14] in grey.

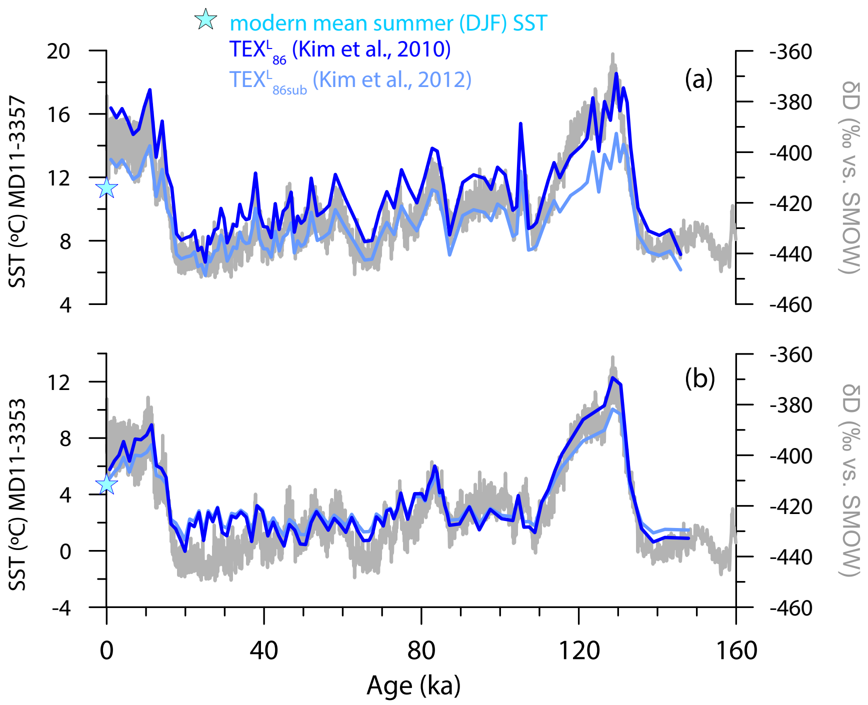

Supplementary Figure 2. Comparison of different calibrations based on the TEX^{L}_{86} index for cores (a) MD11–3357 (SAZ) and (b) MD11–3353 (AZ) compared to the EDC δD record[14] in grey.

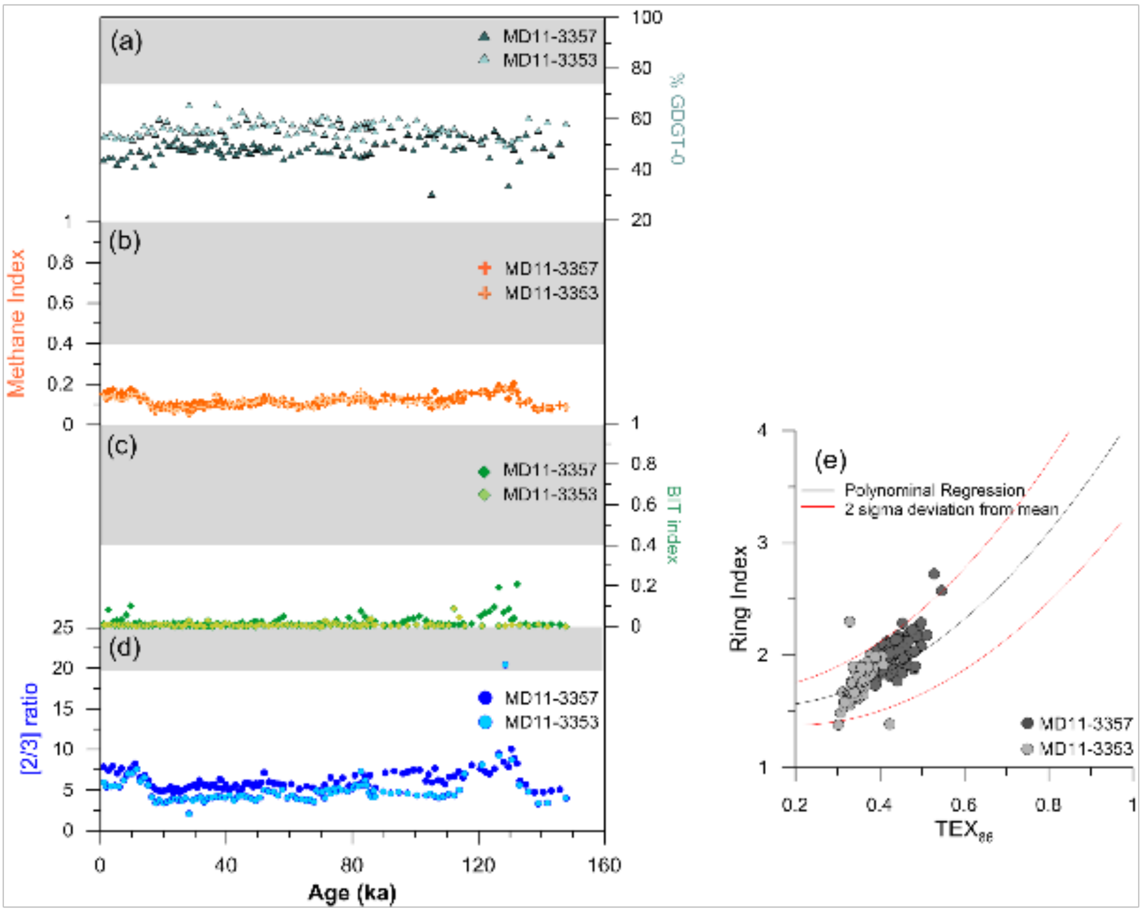

Supplementary Figure 3. Comparison of different GDGT-based indices. a) % GDGT-0 (relative production of GDGT-0, produced by archea living under anoxic conditions)[8], b) MI-index (relative influence of methanotrophic bacteria)[6], c) BIT (branched vs tetraether index, relative input of terrestrial material, as branched GDGTs are produced by soil bacteria)[7], d) [2/3] ratio (indicative for the depth of production)[9] and e) Ring index (deviations from modern analogues of the TEX_{86}-inferred temperatures)[10] for cores MD11–3357 and MD11–3353.

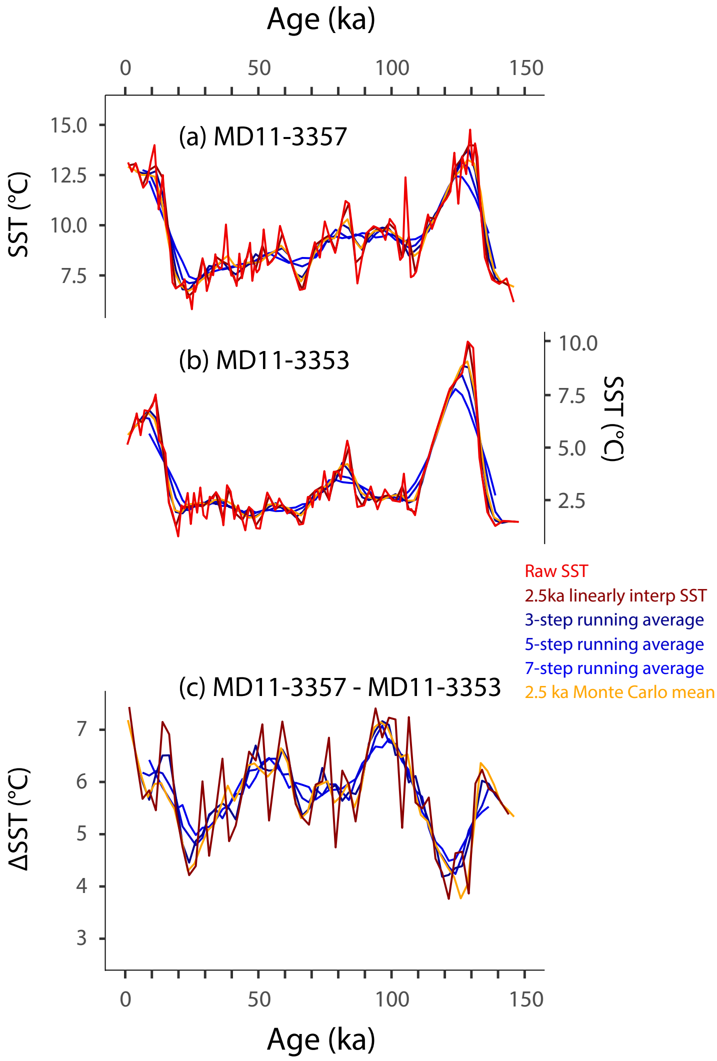

Supplementary Figure 4. Comparison of different resampling methods for (a) the SAZ core MD11–3357 and (b) the AZ core MD11–3353, and (c) the ΔSST. Shown are the raw SST reconstructions, the 2,500-year linear interpolation, the running average for 3, 5 and 7 steps and the Monte Carlo Kalman filter mean SST calculation.

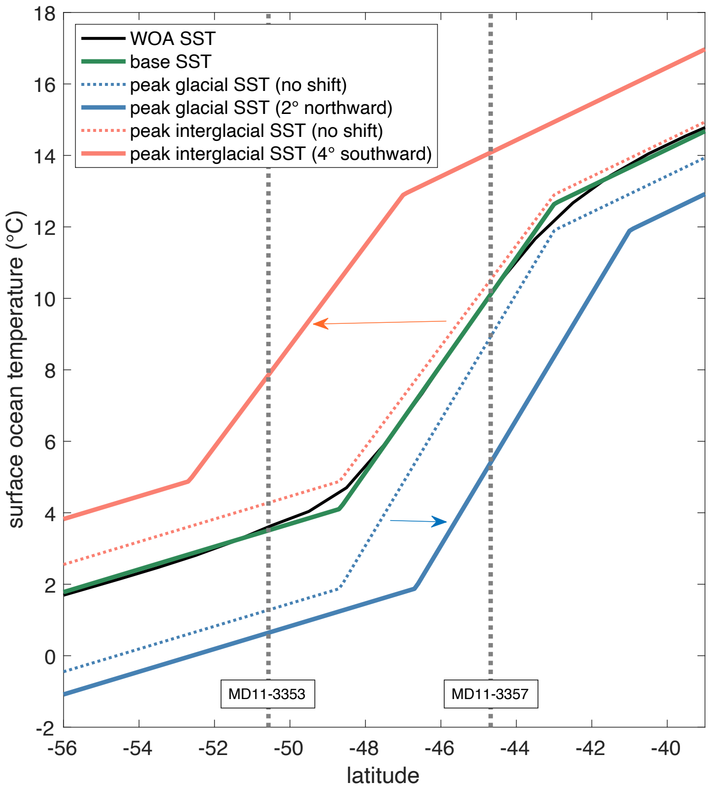

Supplementary Figure 5. Schematic of the SST profiles in the quantitative framework. The black curve is the zonally averaged mean summer temperatures of 0-200m depth of the region 68.5°E to 80.5°E, 34.5°S to 60.5°S from World Ocean Atlas (WOA) 2018[3]. Green lines are the simplified three segments (from south to the north: AZ, PFZ and SAZ) of the WOA2018 SST. Blue and red dotted lines are the simulated peak glacial SST and peal interglacial SST respectively if there is no frontal shift. Blue and red solid lines are the simulated peak glacial SST and peal interglacial SST respectively if there is frontal shift. In this schematic, we are only showing the case in which the modern SST is the initial scenario, and the maximum temperature change range for the AZ ($range_{AZ}$) and SAZ ($range_{SAZ}$) are 3°C and 1°C respectively. The 2° northward shift and 4° southward shift of the SST profiles are only to demonstrate the effect of frontal shifts, and these values are not the actual simulated amount of frontal shifts for peak glacial and peak interglacial periods.

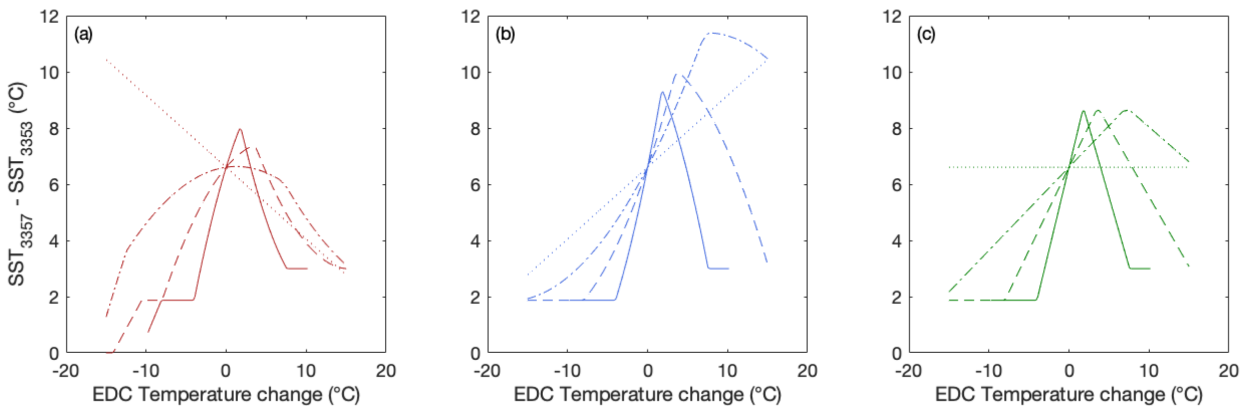

Supplementary Figure 6. Simulated SST gradients between the two core sites plotted over EDC temperature change for different scenarios. (a) $range_{AZ} = 5$, $range_{SAZ} = 0$; (b) $range_{AZ} = 0$, $range_{SAZ} = 5$; (c) $range_{AZ} = 0$, $range_{SAZ} = 0$. In all three subplots, solid line represents $\Delta lat =$

ΔT_{EDC}, dashed line represents Δlat = 0.5*ΔT_{EDC}, dash-dotted line represents Δlat = 0.25*ΔT_{EDC}, dotted line represents Δlat = 0.

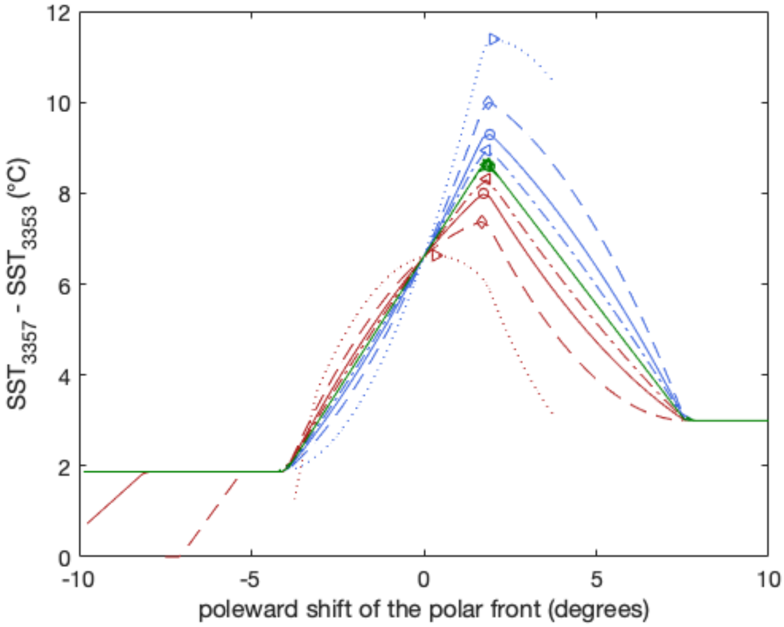

Supplementary Figure 7. Simulated SST gradients between the two core sites plotted over the amount of polar frontal shift for different scenarios. Red represents $range_{AZ}$ = 5, $range_{SAZ}$ = 0; blue represents $range_{AZ}$ = 0, $range_{SAZ}$ = 5; green represents $range_{AZ}$ = 0, $range_{SAZ}$ = 0. Solid line represents Δlat = ΔT_{EDC}, dashed line represents Δlat = 0.5*ΔT_{EDC}, dash-dotted line represents Δlat = 2*ΔT_{EDC}, dotted line represents Δlat = 0.25*ΔT_{EDC}. Open markers represent the maximum simulated SST gradient (circle: $\Delta lat = \Delta T_{EDC}$; diamond: $\Delta lat = 0.5 * \Delta T_{EDC}$; left triangle: $\Delta lat = 2 * \Delta T_{EDC}$; right triangle: $\Delta lat = 0.25 * \Delta T_{EDC}$).

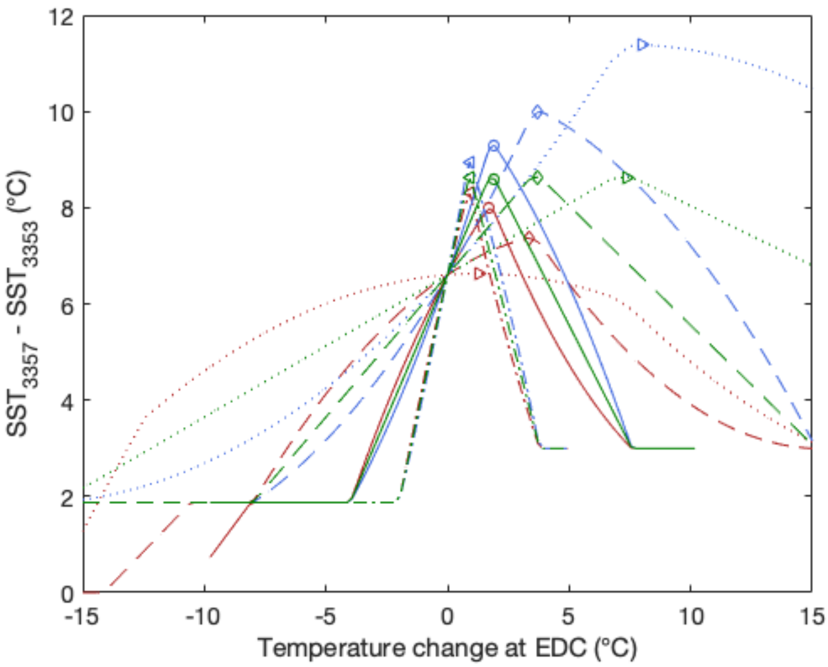

Supplementary Figure 8. Simulated SST gradients between the two core sites plotted over temperature change at EDC for different scenarios. Red represents $range_{AZ}$ = 5, $range_{SAZ}$ = 0;

blue represents $range_{AZ}$ = 0, $range_{SAZ}$ = 5; green $range_{AZ}$ = 0, $range_{SAZ}$ = 0. Solid line represents $\Delta lat = \Delta T_{EDC}$, dashed line represents Δlat = 0.5*ΔT_{EDC}, dash-dotted line represents Δlat = 2*ΔT_{EDC}, dotted line represents Δlat = 0.25*ΔT_{EDC}. Open markers represent the maximum simulated SST gradient (circle: $\Delta lat = \Delta T_{EDC}$; diamond: $\Delta lat = 0.5 * \Delta T_{EDC}$; left triangle: $\Delta lat = 2 * \Delta T_{EDC}$; right triangle: $\Delta lat = 0.25 * \Delta T_{EDC}$).

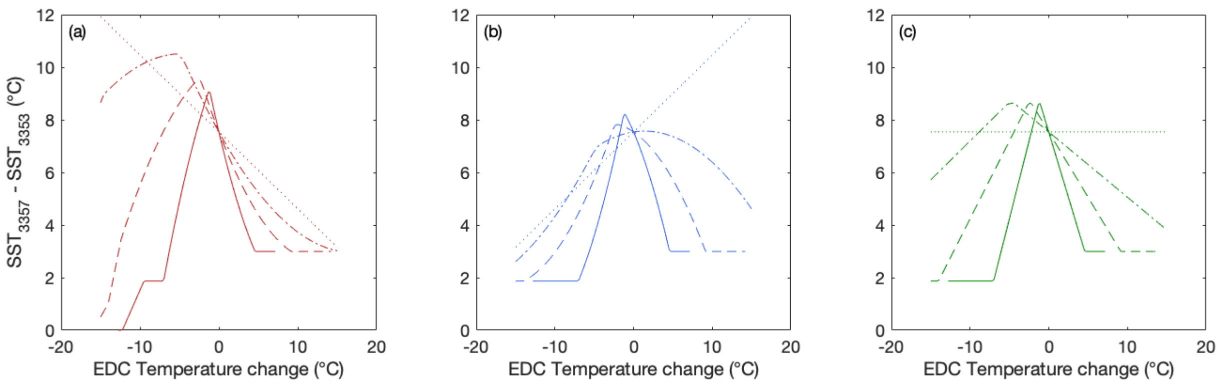

Supplementary Figure 9. Simulated SST gradients between the two core sites plotted over EDC temperature change for different scenarios. (a) $range_{AZ}$ = 5, $range_{SAZ}$ = 0; (b) $range_{AZ}$ = 0, $range_{SAZ}$ = 5; (c) $range_{AZ}$ = 0, $range_{SAZ}$ = 0. In all three subplots, solid line represents $\Delta lat = \Delta T_{EDC}$ +3, dashed line represents Δlat = 0.5* ΔT_{EDC} +3, dash-dotted line represents Δlat = 0.25*ΔT_{EDC}+3, dotted line represents Δlat = 3.

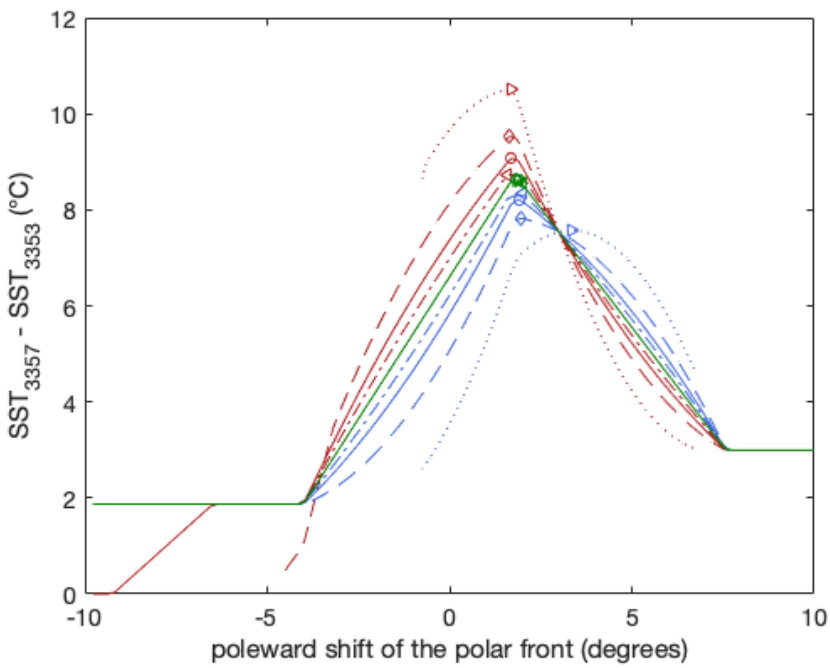

Supplementary Figure 10. Simulated SST gradients between the two core sites plotted over the amount of polar frontal shift for different scenarios. Red represents $range_{AZ}$ = 5, $range_{SAZ}$ = 0; blue represents $range_{AZ}$ = 0, $range_{SAZ}$ = 5; green $range_{AZ}$ = 0, $range_{SAZ}$ = 0. Solid line represents $\Delta lat = \Delta T_{EDC}$+3, dashed line represents Δlat = 0.5*ΔT_{EDC}+3, dash-dotted line represents Δlat = 2*ΔT_{EDC}+3, dotted line represents Δlat = 0.25*ΔT_{EDC}+3. Open markers represent the maximum simulated SST gradient (circle: $\Delta lat = \Delta T_{EDC}$; diamond: $\Delta lat = 0.5 * \Delta T_{EDC}$; left triangle: $\Delta lat = 2 * \Delta T_{EDC}$; right triangle: $\Delta lat = 0.25 * \Delta T_{EDC}$).

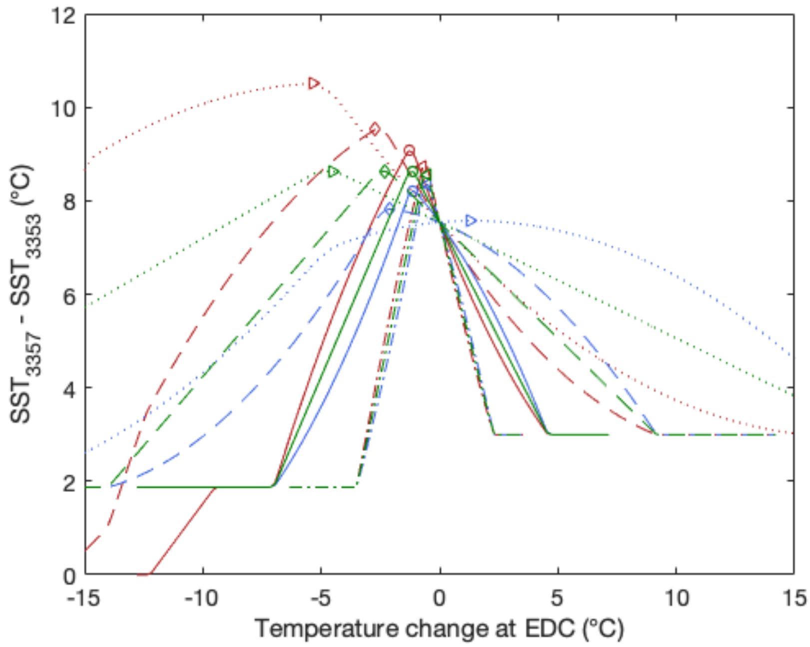

Supplementary Figure 11. Simulated SST gradients between the two core sites plotted over temperature change at EDC for different scenarios. Red represents $range_{AZ}$ = 5, $range_{SAZ}$ = 0; blue represents $range_{AZ}$ = 0, $range_{SAZ}$ = 5; green $range_{AZ}$ = 0, $range_{SAZ}$ = 0. Solid line represents Δlat = ΔT_{EDC}, dashed line represents Δlat = 0.5* ΔT_{EDC} +3, dash-dotted line represents Δlat = 2*ΔT_{EDC}+3, dotted line represents Δlat = 0.25*ΔT_{EDC} +3. Open markers represent the maximum simulated SST gradient (circle: $\Delta lat = \Delta T_{EDC}$; diamond: $\Delta lat = 0.5 * \Delta T_{EDC}$; left triangle: $\Delta lat = 2 * \Delta T_{EDC}$; right triangle: $\Delta lat = 0.25 * \Delta T_{EDC}$).

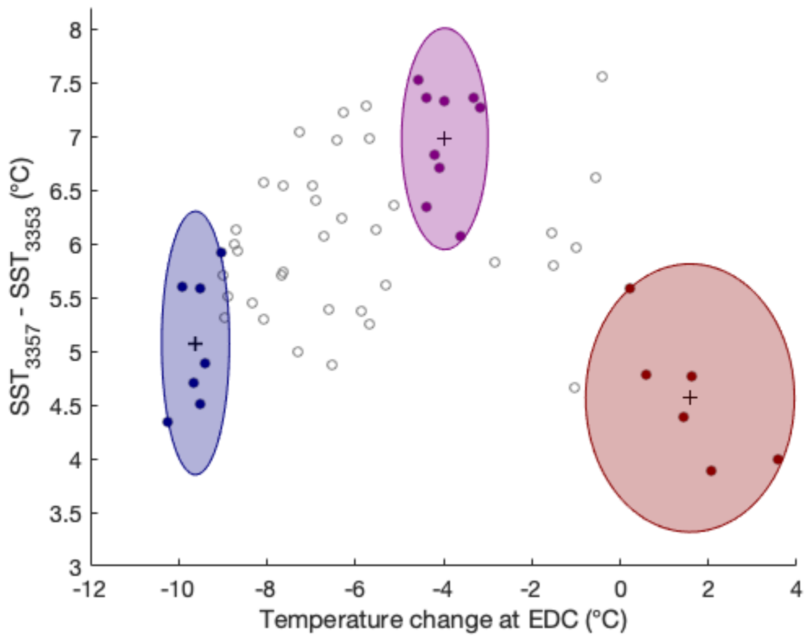

Supplementary Figure 12. **Reconstructed ΔSST plotted over temperature change at EDC**. Dark blue circles are peak glacial data (EDC temperature change < -9°C) and dark red circles are peak interglacial data (EDC temperature change > 0°C). The purple circles are data with EDC temperature change between -5°C and -3°C. The corresponding ellipses represent the mean and 95% confidence (2 std) of the three groups of data.

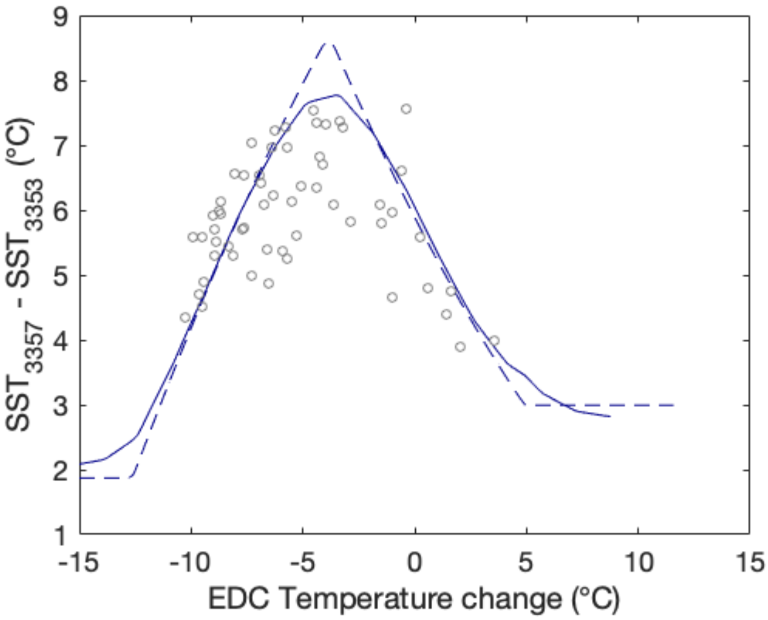

Supplementary Figure 13. **Reconstructed TEX^{L}_{86}-SST gradients (gray circles) and model-simulated SST gradients with optimal parameters (deep-blue lines) between MD11-3353 and the MD11-3357 plotted over temperature change at EDC**. Dashed line is the simulation with the simplified three-segment SST lines, and the solid line is the simulation taking into account the curvature in the SST change at the boundaries between the different zones.

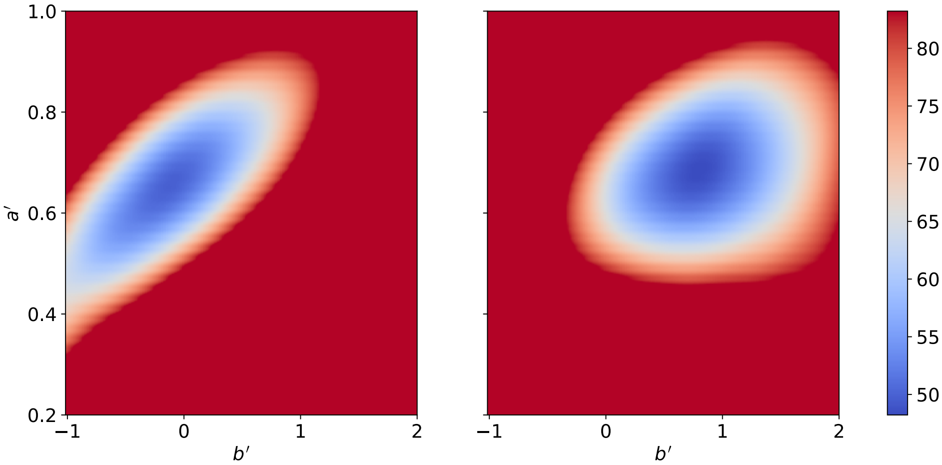

Supplementary Figure 14. Optimization of the parameters $\boldsymbol{a'}$ and $\boldsymbol{b'}$. Color-scale represent the cost-function (a representation of the difference between the reconstructed data and the output of the model) for different combinations of a' and b', when $range_{AZ}$ = 3°C, and $range_{SAZ}$ = 1°C (left) and when $range_{AZ}$ = 1°C, and $range_{SAZ}$ = 3°C (right).

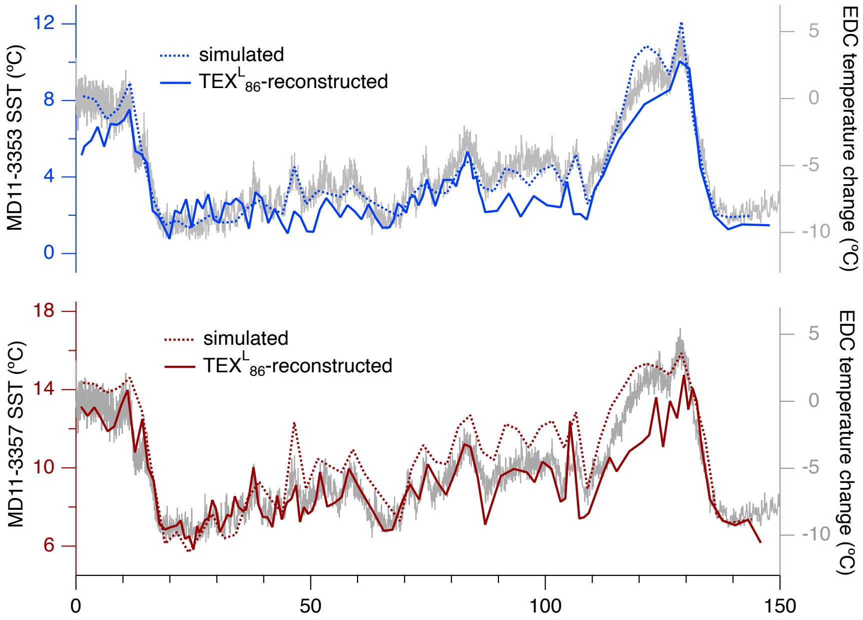

Supplementary Figure 15. Comparison of TEX$^L_{86}$-reconstructed SST and simulated SST at MD11-3353 and MD11-3357 during the last 150,000 years. Solid lines represent TEX$^L_{86}$-reconstructed SST, and dotted lines represent SST simulated with the optimized parameters ($range_{AZ}$ = 3, $range_{SAZ}$ = 1, a'= 0.66, and b'= −0.11).

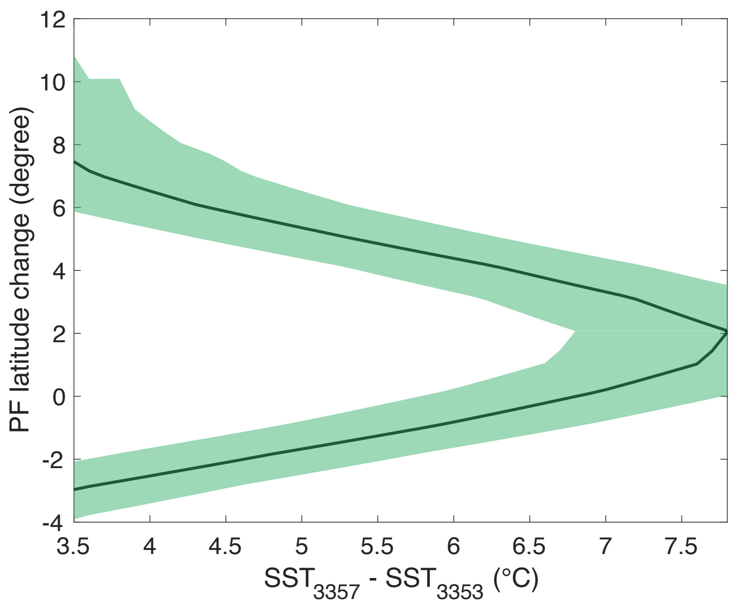

Supplementary Figure 16. Modelled relationship between SST gradient and PF latitude change. The green shading represents the 68% confidence interval of the predicted PF change, assuming that the SST gradient has a standard deviation of 1°C.

Supplementary references

1. Kim, J.-H. *et al.* New indices and calibrations derived from the distribution of crenarchaeal isoprenoid tetraether lipids: Implications for past sea surface temperature reconstructions. *Geochimica et Cosmochimica Acta* **74**, 4639–4654 (2010).
2. Kim, J.-H. *et al.* Holocene subsurface temperature variability in the eastern Antarctic continental margin. *Geophysical Research Letters* **39**, (2012).
3. Locarnini, M. *et al.* World Ocean Atlas 2018, Volume 1: Temperature. (2018).
4. Ho, S. L. *et al.* Appraisal of TEX86 and TEX86L thermometries in subpolar and polar regions. *Geochimica et Cosmochimica Acta* **131**, 213–226 (2014).
5. Tierney, J. E. *et al.* Late-twentieth-century warming in Lake Tanganyika unprecedented since AD 500. *Nature Geosci* **3**, 422–425 (2010).
6. Zhang, Y. G. *et al.* Methane Index: A tetraether archaeal lipid biomarker indicator for detecting the instability of marine gas hydrates. *Earth and Planetary Science Letters* **307**, 525–534 (2011).
7. Hopmans, E. C. *et al.* A novel proxy for terrestrial organic matter in sediments based on branched and isoprenoid tetraether lipids. *Earth and Planetary Science Letters* **224**, 107–116 (2004).
8. Sinninghe Damsté, J. S., Ossebaar, J., Schouten, S. & Verschuren, D. Distribution of tetraether lipids in the 25-ka sedimentary record of Lake Challa: extracting reliable TEX86 and MBT/CBT palaeotemperatures from an equatorial African lake. *Quaternary Science Reviews* **50**, 43–54 (2012).
9. Hernández-Sánchez, M. T. *et al.* Further insights into how sediment redox status controls the preservation and composition of sedimentary biomarkers. *Organic Geochemistry* **76**, 220–234 (2014).
10. Zhang, Y. G., Pagani, M. & Wang, Z. Ring Index: A new strategy to evaluate the integrity of TEX86 paleothermometry. *Paleoceanography* **31**, 220–232 (2016).
11. Wang, X. T. *et al.* Deep-sea coral evidence for lower Southern Ocean surface nitrate concentrations during the last ice age. *Proc Natl Acad Sci USA* **114**, 3352–3357 (2017).
12. Kohfeld, K. E. & Chase, Z. Temporal evolution of mechanisms controlling ocean carbon uptake during the last glacial cycle. *Earth and Planetary Science Letters* **472**, 206–215 (2017).
13. Waelbroeck, C. *et al.* Constraints on the magnitude and patterns of ocean cooling at the Last Glacial Maximum. *Nature Geosci* **2**, 127–132 (2009).
14. Jouzel, J. *et al.* Orbital and Millennial Antarctic Climate Variability over the Past 800,000 Years. *Science* **317**, 793–796 (2007).